Progress in PHOTOVOLTAICS

PROGRESS IN PHOTOVOLTAICS: RESEARCH AND APPLICATIONS
Prog. Photovolt: Res. Appl. 2016; **24:**446–457
Published online 6 November 2014 in Wiley Online Library (wileyonlinelibrary.com). DOI: 10.1002/pip.2559

29TH EU PVSEC, AMSTERDAM, THE NETHERLANDS 2014

Comparison of amorphous silicon absorber materials: Kinetics of light-induced degradation

Michael Stuckelberger*, Adrian Billet, Yannick Riesen, Mathieu Boccard, Matthieu Despeisse, Jan-Willem Schüttauf, Franz-Josef Haug and Christophe Ballif

Ecole Polytechnique Fédérale de Lausanne (EPFL), Institute of Microengineering (IMT), Photovoltaics and Thin-Film Electronics Laboratory, Rue de la Maladière 71, CH-2000 Neuchâtel, Switzerland

ABSTRACT

We investigate the influence of the deposition parameters for intrinsic amorphous silicon absorber layers on light-induced degradation (LID) of thin-film silicon solar cells. The focus is on absorber layers with different bandgaps: on one side, solar cells with a wide-bandgap absorber layer that provides open-circuit voltages up to 1.04 V; on the other, cells with short-circuit current densities of 18.2 mA / cm^2 with a 300-nm-thick narrow-bandgap absorber layer, and 20 mA / cm^2 at reverse bias for a cell with a 1000-nm-thick absorber layer. Between these extremes, we varied the hydrogen-to-silane ratio and the deposition pressure during the absorber layer deposition. The light-induced degradation of these materials—covering the deposition regimes of low-pressure, protocrystalline, polymorphous, and high-pressure amorphous silicon—incorporated in single-junction amorphous silicon solar cells is detailed here. For each pressure, we found an optimum hydrogen dilution with least LID close to the amorphous-to-microcrystalline transition. The relative LID is similar for all pressures at optimized hydrogen dilutions. Further, we present the influence of absorber layer thickness, *p*-layer thickness, and deposition rate on the kinetics of light-induced degradation to facilitate the choice of a material for its application in several types of multi-junction thin-film silicon solar cells. We show that the degradation kinetics depends, in semi-logarithmic scale, only weakly on time but more on deposition conditions. Copyright © 2014 John Wiley & Sons, Ltd.

KEYWORDS

solar cells; a-Si:H; amorphous silicon; Staebler-Wronski effect; light-induced degradation; degradation kinetics; narrow bandgap; wide bandgap

***Correspondence**

Michael Stuckelberger, Ecole Polytechnique Fédérale de Lausanne (EPFL), Institute of Microengineering (IMT), Photovoltaics and Thin-Film Electronics Laboratory, Rue de la Maladière 71, CH-2000 Neuchâtel, Switzerland.
E-mail: michael.stuckelberger@epfl.ch

Received 30 June 2014; Revised 1 September 2014; Accepted 9 September 2014

1. INTRODUCTION

Nearly 40 years after the discovery of light-induced degradation (LID) of amorphous silicon (*a*-Si:H) and its partial reversibility by thermal annealing, this so-called Staebler-Wronski effect [1] is still not fully understood, although several models exist for its explanation [2–5]; of particular importance are the "weak-bond model" [6], the "H-collision model" [7], and Smets' model with divacancies playing an important role [5].

Following a degradation of about 8 – 10% for the most stable materials [8,9], the highest stabilized efficiencies are about 10% for single-junction *a*-Si:H solar cells after light soaking [10,11]. To understand the processes of light-induced defect generation and thermal annealing, studies of LID kinetics were typically conducted on layers, and M. Stutzmann *et al.* found experimentally (based on electron spin resonance measurements of the neutral dangling bonds) in agreement with the "weak-bond model" [12] the dependence of the dangling bond concentration N_{db}

$$N_{\mathrm{db}}(t) \propto G^{\frac{2}{3}} \cdot t^{\frac{1}{3}}, \tag{1}$$

on the time t and on the electron–hole pair generation rate G. (After correction for initial dangling bonds, Deng *et al.* found rather $N_{\mathrm{db}}(t) \propto G \cdot t^{\frac{1}{2}}$ for protocrystalline silicon) [13].

The defect density was found to saturate at an equilibrium dangling bond density $N_{\mathrm{db}}^{\mathrm{eq}} \propto G^{\frac{1}{3}}$. This justifies the terminology of "stabilized defect density" if this equilib-

rium state is reached after light soaking. However, in solar cells, we typically observe a continuing degradation within the investigated time of 1000 h under one sun and 24 h under three sun light-soaking; the degradation is approximately linear in semi-logarithmic scale as will be shown in the following sections. Because of the ongoing light-induced degradation, we avoid the term "stabilized" to describe solar cell performance after light-soaking.

The correlation between dangling bond density and fill factor (*FF*) or other parameters measured directly on solar cells is not direct. Therefore, we propose that a correlation of experimental solar cell degradation kinetics data with a defect-density generation model is not appropriate.

In this contribution, we focus on the kinetics of LID for high efficiency single-junction *a*-Si:H solar cells that have different absorber layers, while keeping the rest of the solar cell structure as constant as possible. This experimental comparison not only helps us to relate the deposition conditions with LID but also allows us to determine which absorber material is best suited for a given application.

After detailing the experimental setups and processes in Section 2, we present solar cells with a wide-bandgap absorber layer providing open-circuit voltages (V_{oc}) up to 1.04 V (Section 3) and with a narrow-bandgap absorber layer providing short-circuit current densities (J_{sc}) well above 18 mA / cm^2 (Section 4). The absorber layers used in these solar cells mark the two extremes of the bandgap for intrinsic amorphous silicon (*i*) that still provide good electrical properties in solar cells. These materials are of special interest for applications in multi-junction solar cells.

In Section 5, we give a quantitative overview regarding degradation for *a*-Si:H materials deposited at different pressures and hydrogen-to-silane ratios (hydrogen dilutions) for highly efficient single-junction *a*-Si:H devices, and show degradation kinetics measurements for a hydrogen-dilution series. In the following sections, we focus on the impact of further deposition parameters on LID kinetics: we alternate the deposition rate by plasma power in Section 6 and the thickness of the boron-doped amorphous silicon carbide (*p*-(*a*-SiC:H)) layer in Section 7. Finally, we compare polymorphous [14,15] (*pm*-Si:H) with *a*-Si:H absorber layers in Section 8.

2. EXPERIMENTAL

2.1. Solar cell design

All solar cells presented in this study were made in the *p-i-n* configuration (superstrate) on boron-doped zinc-oxide (ZnO:B) grown by low-pressure chemical vapor deposition (LPCVD) as the front electrode. We treated these substrates partially with an argon plasma to smoothen the surface texture [16].

As the back electrode, 2.3-μm-thick LPCVD ZnO:B was used for all cells except those presented in Section 8, where metallic back electrodes were used.

The silicon layers of the solar cells described in Sections 4–7 were grown by plasma-enhanced chemical vapor deposition in a cluster tool (Octopus I from INDEOtec SA) [17] with dedicated chambers for *p*-type, *n*-type, and intrinsic layers, described elsewhere [18]. The solar cells described in Section 3 were deposited in a two-chamber plasma-enhanced chemical vapor deposition system built in-house.

The *p-i-n* junctions include *p*-type and *n*-type microcrystalline silicon oxide layers, *p*-(μc-SiO:H) and *n*-(μc-SiO:H), in direct contact with the front and back ZnO for good electrical contact, transparency, and shunt-quenching [19,20]. At the *p-i* interface, we used a boron-doped amorphous silicon carbide layer, *p*-(*a*-SiC:H) and an intrinsic amorphous silicon buffer layer; to widen its bandgap, carbon or oxygen [21] was added in some cases. After the absorber layer, we deposited a phosphorus-doped *a*-Si:H layer at the *i-n* interface.

Except for the *i*-layer thickness series in Section 4, the *i*-layers were always 220 nm thick (*i*-layer thicknesses are given as nominal thicknesses on flat substrates).

As precursor gases for the intrinsic *a*-Si:H absorber layers, only silane (SiH_4) and hydrogen (H_2) were used. More details about individual layers, the reactor, and gas precursors are published elsewhere [18,22].

Finally, solar cells were defined by a combination of wet and dry etching. The size is typically 0.25 cm^2 unless specified otherwise.

For all solar cell series presented here, the baseline process provided initial solar cell efficiencies above 10%.

2.2. Measurements

Current–voltage $I(V)$ characteristics were measured under a four-lamp (three halogen, one xenon) solar simulator from Wacom (class AAA) under standard conditions (AM1.5g, 1000 W / m^2, 25 °C) [23,24]. The current density was determined from external quantum efficiency (*EQE*) measurements, performed with a system built in-house. A diffusing white back reflector made from polytetrafluoroethylene was used during measurement.

Light soaking of the solar cells described in Section 5 was performed in a solar simulator from Solaronix (class AAA) for 1000 h at 50 °C under 1000 W / m^2 of AM1.5g, a common standard derived from the international norms [24,25]. The solar cell in the center of the substrate that performed best after light soaking was used for the presented analysis.

For *in situ* measurement of the LID kinetics, the solar cells were contacted by ultrasonic soldering. These measurements were performed at three sun equivalents for about 24 h at 50 °C, for which a dedicated solar simulator [26], fully based on light-emitting diodes and built in-house, was used. Such light-soaking conditions leading to accelerated degradation reduce the feedback time in solar cell optimization significantly. In the present case, it also allowed the measurement of the degradation kinetics of several solar cell series within a few weeks rather than

within months; preliminary measurements showed that the light soaking for 24 h at 50 °C and three sun equivalent corresponds roughly to light soaking for 1000 h at 50 °C and 1 sun equivalent. While the *in situ* measurement of the $I(V)$ curves in the light-soaking system enables the fully automated tracking of the cell performance without substrate manipulation, the solar cell parameters change considerably with increased light-intensity and temperature. This is particularly true for the *FF* that is reduced by enhanced resistive losses and recombination.

Solar cell series were always light soaked simultaneously for a fair comparison (except the different substrate roughnesses in Section 7, Figure 11b). Therefore, experimental issues like temperature instability of the environment that induced instabilities in light-emitting diode illumination (seen, e.g., as instabilities of $I(V)$ curve measurements) were the same for all solar cells shown in the same graph. To check reproducibility, we always tracked the performance of three to four cells on the same substrate. In Figures 11a and 12, we show the results of several cells per substrate, everywhere else only one that is typical for the sake of clarity. Dots present single measurements, lines are smoothed.

3. WIDE BANDGAP FOR HIGH VOLTAGES

Amorphous silicon solar cells with a wide-bandgap absorber layer were recently used as top cells in quadruple-junction solar cells [27] and are regularly used as top cells in triple-junction solar cells [28,29], which currently hold the world record for thin-film silicon solar cell technology [30,31].

For such applications, we developed wide-bandgap *a*-Si:H materials by increasing the hydrogen dilution close to the transition to microcrystalline silicon and slightly lowering the deposition temperature. Incorporating this material as an absorber layer in solar cells that were optimized for narrower-bandgap absorbers provides more than 1 V V_{oc} with a *FF* of 71% on smooth substrates (measured under standard conditions) (Figure 1). Under very low illumination (4 W / cm^2), this cell still provides 760 mV, which makes it interesting for powering small electronic circuits, for example, for indoor applications. Optimization of the doped and buffer layers for cells with a wide-bandgap absorber layer would probably further increase the V_{oc}. The maximum V_{oc} we obtained using narrow-bandgap absorber layers was 1.04 *V*; the maximum $V_{oc} \times FF$ product was 739 mV. Note that these results were obtained with absorber layers deposited from H_2/SiH_4 mixtures without use of bandgap-widening elements such as oxygen or carbon.

In addition to hydrogen dilution, on which we focus in Section 5, the deposition temperature has a major impact on the bandgap. Therefore, we investigate the degradation kinetics of solar cells for which the deposition temperature was varied from 140 to 200 °C. In this series, the temperature was kept the same for all layers of the stack, including the doped layers. Different from the variation of the absorber layer deposition conditions in the remainder of this study, this has the advantage that hydrogen effusion from the absorber layer (accompanied by bandgap reduction) during the deposition of subsequent layers at higher temperatures should not be an issue, and the bandgap mismatch between doped layers and the absorber layer is kept small, as the bandgap changes of doped and intrinsic layers with temperature show the same trends. However, it means that differences between solar cells cannot simply be ascribed to absorber layer effects.

Figure 2c shows the V_{oc} degradation kinetics of this series during light soaking at three sun equivalent light intensity and 50 °C. The solar cell with $I(V)$ characteristics shown in Figure 1 was co-deposited at 180 °C with the cells presented here, but on a flatter substrate. Because of issues with ultrasonic soldering on flat substrates, we show in this analysis cells co-deposited on a rougher substrate type.

As expected, the V_{oc} increases with decreasing deposition temperature due to wider bandgaps. However, the V_{oc} of the cells deposited at very low temperatures decreases again, not because of the bandgap but because of higher defect density, which is reflected in significantly lower *FF* as shown in Figure 2d.

Both V_{oc} and *FF* show two regions with different slopes in logarithmic scale with a change after a few hours, which could indicate two distinct degradation mechanisms as concluded elsewhere [32], where "fast" degradation in the beginning was attributed to nanosized voids, and later "slow" degradation to metastable defects. In contrast, here, we observe slow degradation in the beginning and fast degradation afterwards, both in V_{oc} and *FF*. Figure 2a and b shows the light intensity and substrate temperature during light soaking. The light intensity curve seems to

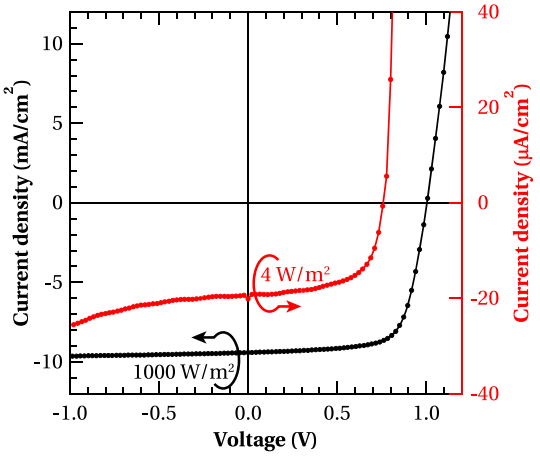

Figure 1. $I(V)$ curve of an amorphous silicon solar cell with V_{oc} above 1 *V* under standard conditions and 760 mV at 4 W / m^2 light intensity, measured using a 0.4% grey transmission filter.

DOI: 10.1002/pip

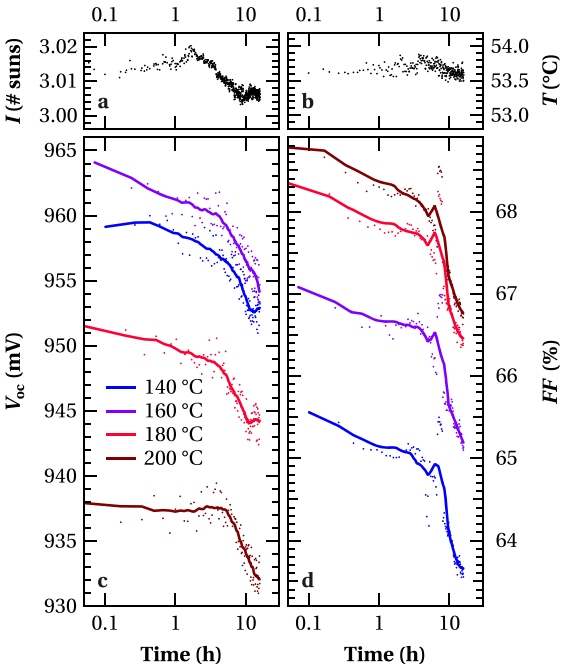

Figure 2. Degradation kinetics of open-circuit voltage (c) and fill factor (d) during light soaking at three sun equivalent light intensity and 50 °C for solar cells deposited at different temperatures, with the light intensity (a) and substrate temperature (b) during light soaking.

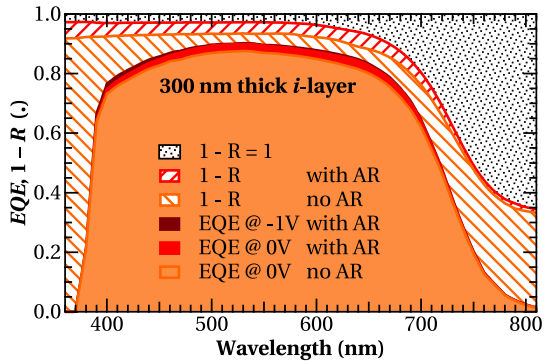

Figure 3. External quantum efficiency and 1 – reflectance measurements of a single-junction *a*-Si:H solar cell providing J_{sc} = 18.19 mA / cm^2.

be correlated with the V_{oc} and *FF* curves, and one could attribute the change of slopes to a measurement effect of instable light intensity. However, the change in the light intensity slope takes place at least 2 h before the V_{oc} and *FF* slope changes. Further, it is questionable whether such small variations of half a percent in intensity can cause such changes in solar cell performance (note the logarithmic dependence of V_{oc} on light intensity). At this point, we do not know the reason for the slope change but will investigate it further.

4. NARROW BANDGAP FOR HIGH CURRENTS

We have developed narrow-bandgap *a*-Si:H materials for application as the absorber layer in the top cell in micromorph tandem solar cells. In this section, we present a thickness series of this material from 120 to 1000 nm, deposited at 230 °C at RF, included in single-junction *a*-Si:H solar cells.

Figure 3 shows *EQE* and 1 – reflectance (1 – *R*) measurements of the solar cell with a 300-nm-thick absorber layer; the J_{sc} and measurement conditions are summarized in Table I, along with results from a solar cell with a 1000-nm-thick absorber layer. We emphasize that the doped layers have standard thicknesses as reported elsewhere [22].

The solar cell with a 300-nm-thick absorber layer provide 880 mV V_{oc} and 72% *FF* (0.25 cm^2 cells). Current densities were measured on co-deposited 1 cm^2 cells for more correct current measurement on rough substrates.

We achieved short-circuit current densities of 18.19 mA / cm^2 for solar cells with a 300-nm-thick absorber layer and pyramids providing geometrical light trapping [33] glued on the front glass (AR). The solar cell with a 1000-nm-thick absorber layer provides even higher short-circuit current densities of 19.51 mA / cm^2 and shows the potential to achieve more than 20 mA / cm^2 by applying a reverse bias voltage. These short-circuit current densities are among the highest reported from single junction *a*-Si:H solar cells and higher than the current densities of the cells with highest certified efficiency (17.3 mA / cm^2 after light soaking) [10,30]. The *EQE*-based current measurements were confirmed by *I* – *V* measurements using masks.

Such narrow-bandgap materials are of great importance for high current densities and efficiencies in micromorph tandem solar cells [34]—the stronger LID as compared with materials with a wider bandgap is in this case compen-

Table I. Measurement conditions and short-circuit current densities obtained from solar cells with a 300 or 1000-nm-thick absorber layer.

i-layer thickness (nm)	300	300	1000	1000	1000
AR	No	Yes	No	Yes	Yes
Bias voltage (V)	0	0	0	0	-2
J_{sc} (mA / cm^2)	17.69	18.19	18.82	19.51	20.05

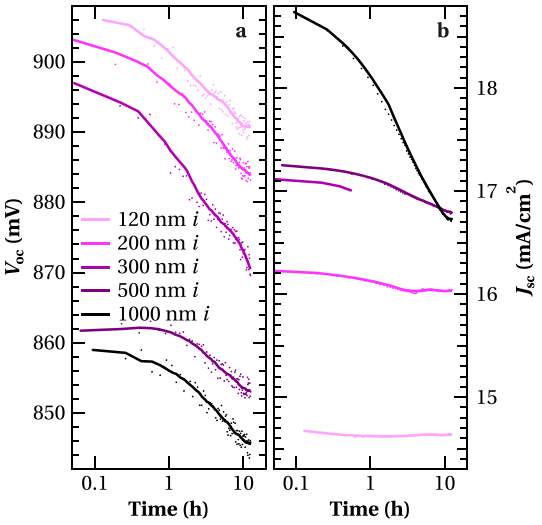

Figure 4. Open-circuit voltage (a) and short-circuit current density (b, normalized to the initial measurements under standard conditions) of a solar cells series with narrow-bandgap absorber layers of different thickness, during light soaking.

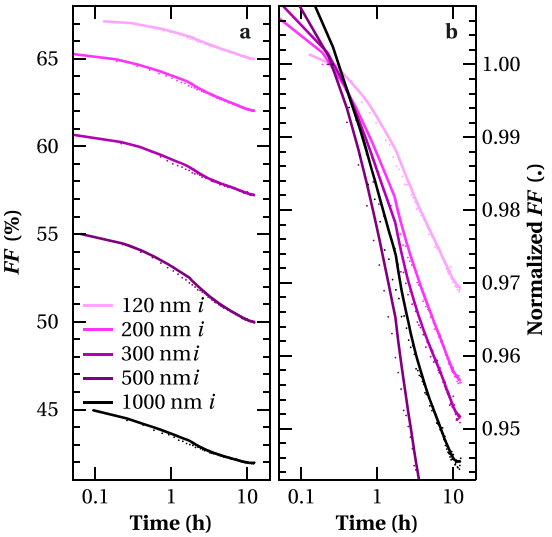

Figure 5. Fill factor in absolute terms (a) and normalized to the first measurement during light soaking (b) of the same solar cells as presented in Figure 4.

sated for by the higher current that allows bottom-limited devices.

Figure 4 shows the degradation kinetics of solar cells with different thicknesses of the narrow-bandgap absorber layer, in terms of V_{oc} and J_{sc}. The current densities were measured during light soaking by $I(V)$ measurements and normalized to the initial currents as determined under standard conditions by *EQE* measurements; the current results for the cell with a 300-nm-thick absorber layer are not shown for the full light soaking time because this substrate detached progressively during light soaking from the cooling unit and heated up, and therefore the current increased stepwise (cf. Figure 10).

Comparing the absolute V_{oc} values, we note that they are lower for thicker substrates due to enhanced recombination. However, the thickness dependence only spans about 50 mV for cells whose absorber thicknesses vary by nearly a factor of 10. For the V_{oc}, the degradation slope is comparable for all *i*-layer thicknesses; this is not the case for the current, where the *i*-layer degradation is more strongly pronounced for thick cells, such that the current densities of the cells with a 1000-nm-thick absorber layer end at values even lower than cells with a thinner absorber layer.

We note the stronger degradation of thicker layers also in the *FF* shown in Figure 5: generally, solar cells with a thick absorber layer suffer from poor charge collection, manifested by a lower *FF* (Figure 5a). The spread of initial *FF* is larger under three sun equivalent illumination intensity than for the standard measurement conditions. One reason is the current that is about three times larger than under one sun illumination. Front and back electrodes were optimized for one sun illumination and thin absorber layers. Hence, the *FF* is significantly limited by series resistance, which is more pronounced for thicker cells and higher illumination.

Thick absorber layers degrade more as shown in Figure 5b by the relative *FF*: thicker *i*-layers lead to a reduction of the charge collection due to a lower electric field that is given in first approximation by the built-in voltage (V_{bi}) divided by the *i*-layer thickness. Enhanced defect density and recombination due to degradation further reduce the electric field in the bulk, which is more detrimental for thicker *i*-layers. This is confirmed and discussed in more detail with an *i*-layer thickness series presented elsewhere [35,36]. The solar cells with a 500-nm-thick absorber layer show even stronger degradation than cells with a 1000-nm-thick absorber layer; in the former case, a plasma problem occurred during buffer layer deposition, which caused probably the unusually strong degradation.

5. THE ROLE OF THE HYDROGEN DILUTION AND PRESSURE

In this section, we present degradation results obtained from solar cell series alternating the H_2:SiH_4 flow ratio over a wide range for four pressure and frequency regimes.

For the best bulk material quality in the different regimes, we chose the lowest excitation power that sustained a stable plasma for all hydrogen dilutions: 3 W at 0.2 and 2.5 mbar, 10 W at 5 mbar, and 20 W at 9 mbar, respectively. We kept the doped layers the same for all cells and added intrinsic *a*-Si:H buffer layers at the *p*-*i* and the *i*-*n* interfaces to further reduce interface phenomena as much as possible. More details about these series are reported elsewhere [18].

DOI: 10.1002/pip

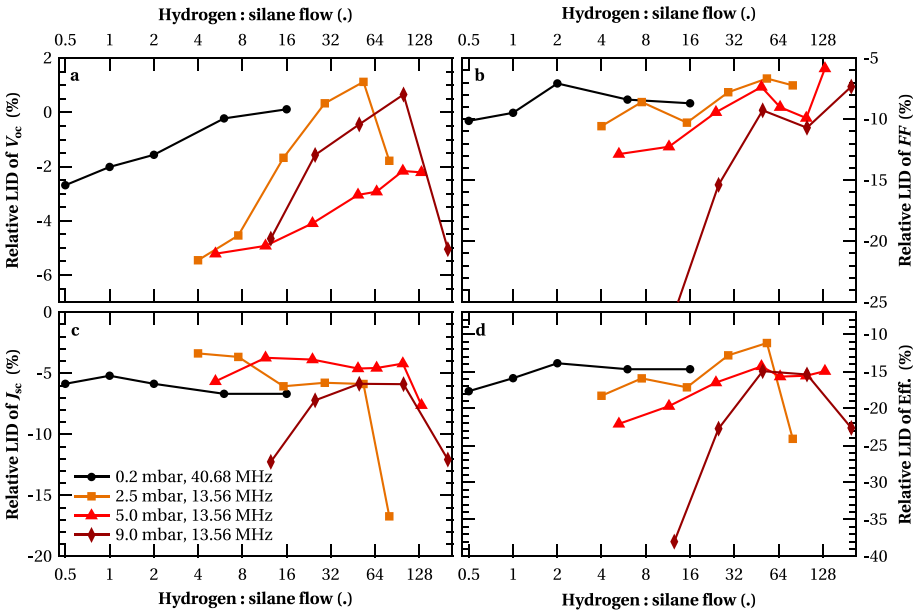

Figure 6. Relative light-induced degradation of the open-circuit voltage (a), fill factor (b), short-circuit current density (c), and conversion efficiency (d) for four series of absorber layers, alternating the hydrogen dilution for different deposition pressures and frequencies.

Figure 6 shows the relative LID $\left(\text{defined as } \Delta X = \frac{X_{\text{after light soaking}} - X_{\text{before light soaking}}}{X_{\text{before light soaking}}}\right)$ of the V_{oc}, FF, J_{sc} and the conversion efficiency for solar cells of these series.

We note:

- V_{oc} degrades less with increasing hydrogen dilution. It can even show an improvement, until a sharp drop occurs at the transition to deposition conditions leading to microcrystalline layers. This is probably linked to lower defect density with increased dilution; detailed discussion is given elsewhere [22]. Already in the initial state, V_{oc} increases strongly with hydrogen dilution due to the wider bandgap. After light soaking, this dependency is reinforced.
- FF degrades less with increasing hydrogen dilution. This is in agreement with the literature, where deposition regimes with highly diluted plasmas close to the transition from amorphous to microcrystalline are reported to provide the most stable materials [37,38].
- There is only a minor effect of hydrogen dilution on J_{sc} degradation, when charge collection gets very poor. Otherwise, the degradation in J_{sc} is mostly due to a loss of transparency in the front ZnO [39].
- The trends observed in conversion efficiency mostly reflect the trends in the FF because this parameter is changing most strongly during light soaking.
- For high pressures, the process window for good solar cells is limited to a certain hydrogen dilution range between powder production at low dilutions leading to poor *a*-Si:H quality and microcrystalline growth at high dilution. This is not the case for low pressures: here, no powder is produced, even without any hydrogen dilution. This leads to comparable relative degradation and higher absolute efficiencies at low dilutions: the higher current due to the narrower bandgap compensates for the lower V_{oc}.
- For all pressure regimes, the lowest relative degradation values are comparable, being around 15% loss in efficiency. This suggests that pressure itself is not a critical parameter for the stability of *a*-Si:H material, but only that the optimum hydrogen dilution is different for each pressure. At least with this reactor and cell design (front/back electrodes, doped and buffer layers, layer thicknesses), it seems that 15% marks the lower limit of relative LID.
- Although the doped layers were neither adapted for record efficiency nor for different *i*-layer process pressures, efficiencies above 7.5% were obtained for each processing pressure and the best cells reached an efficiency of 8.7% with a FF of 68% after light soaking without an anti-reflective coating. With the use of an anti-reflecting coating on larger cells (less scattering of light out of the cell), this corresponds to about 9.5% efficiency.

Using the same cell design as the solar cells presented in Figure 6, we deposited a further hydrogen-dilution series. Here, the absorber layer was deposited at 1 mbar and an excitation frequency of 40.68 MHz.

Figure 7 shows the LID kinetics of the V_{oc} and FF for these solar cells. Same as in the preceding text, the

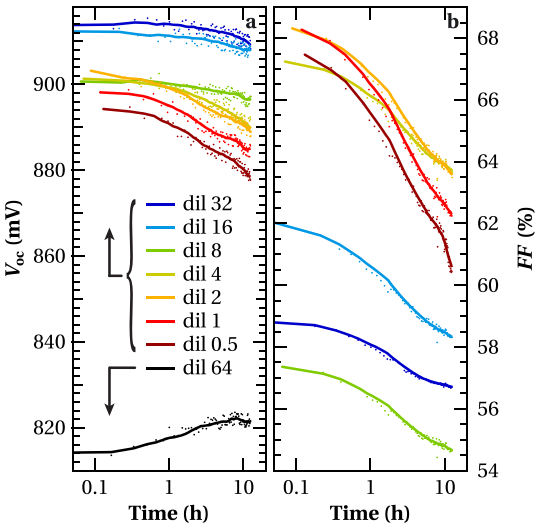

Figure 7. Open-circuit voltage (a) and fill factor (b) of a solar cell series with absorber layers for which the H_2/SiH_4 ratio was increased from 0.5 to 64.

initial V_{oc} increases with hydrogen dilution until it drops when passing the transition to microcrystalline deposition conditions, which takes place between dilutions 32 and 64.

For the *FF*, different effects are visible:

First, the slope of the *FF* degradation is steepest for the lowest dilution and flattest for dilution 32. This is due to the higher initial defect density in low-dilution absorber materials leading to enhanced recombination, hence stronger LID due to the Staebler-Wronski effect.

Second, the initial *FF* is the highest for low hydrogen dilutions (74% measured under standard conditions). A high *FF* in the initial state for low hydrogen dilutions is not unusual, as defect states in the absorber layer are typically not yet limiting. Why the initial *FF* at higher dilutions (8 to 32) are lower is not completely clear; (the cells with an absorber layer deposited with dilution 64 suffered from "S-shaped" *I*(*V*) curves due to the bi-phase material, leading to *FF* below 50%.) We suppose that experimental issues during the *p*-(μc-SiO:H) deposition that suffered from reduced reproducibility at the time this series was deposited, are the cause. Another possible explanation is that the bandgaps of the doped layers are not adapted for the deposition conditions of the absorber layer at high hydrogen dilutions, or that the bombardment of hydrogen-rich plasmas has negative effects on the underlaying buffer and *p*-layers: these layers can be etched by the hydrogen, or hydrogenated which can increase their bandgaps and modify the bandgap mismatch. Using other doped layers, the *FF* with high-dilution *i*-layers can be easily as high as with low-dilution *i*-layers. We were able to confirm this by the implementation of the best-performing absorber layers of each pressure regime shown in Figure 6 into cells with other doped layers; the initial *FF* was there very close and relative degradation performed similarly as shown here.

6. THE ROLE OF THE DEPOSITION RATE

In this section, we investigate the role of the deposition rate on the LID. The most direct impact on the deposition rate comes from the excitation power—at least for the chosen deposition conditions, the impact of excitation power on other parameters such as bandgap is minor—and the relationship is linear within the investigated range as shown in Figure 8 for the absorber layers that will be investigated in this section.

In Figure 9, we compare the V_{oc} of two power series, where we varied the plasma power of the 220-nm-thick absorber layer from 4 to 80 W at two frequencies, corresponding to the deposition rates given in Figure 8.

The deposition pressure was 0.4 mbar for the depositions at 13.56 MHz. For 40.68 MHz, we chose 0.13 mbar. No H_2 dilution was used for the absorber layers; nevertheless, these plasma conditions—using low power and

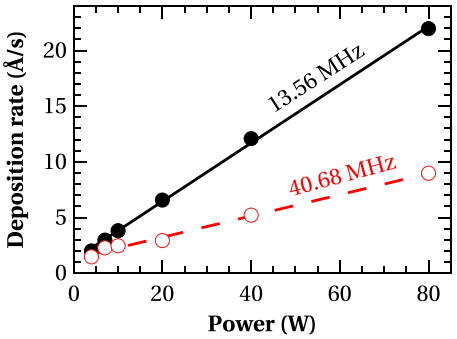

Figure 8. Deposition rate of the absorber layers used in the solar cells presented in Figure 9 and 10. The lines are linear fits.

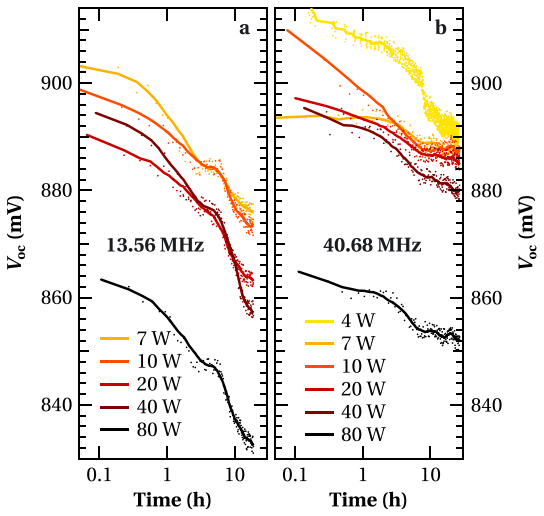

Figure 9. Open-circuit voltage of cells with an absorber layer for which the deposition rate was varied via the power at 13.56 (a) and 40.68 MHz (b).

DOI: 10.1002/pip

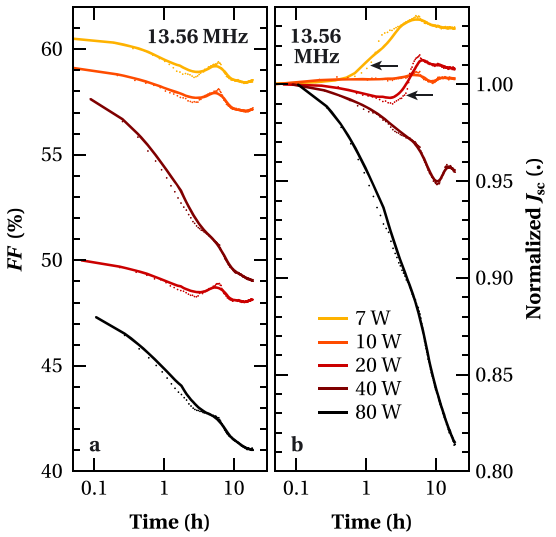

Figure 10. Fill factor and normalized short-circuit current density of the cells shown in Figure 9 with the absorber layer deposited at 13.56 MHz.

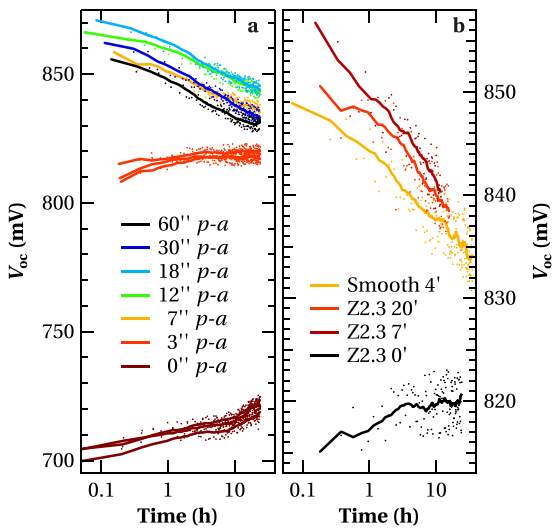

Figure 11. Open-circuit voltage degradation kinetics for cells with different *p*-layer thicknesses, parametrized by the deposition time (a) and for cells deposited on substrates with increasing substrate roughness from Smooth 4′ to Z2.3 0′ (b).

pressure—lead to high-efficiency solar cells as shown in section 4.

High deposition rates lead to high defect density in the absorber layers [6,12,40]. Hence, the V_{oc} should decrease with increasing power, which we see for both frequencies. The degradation rate seems to be independent of the power, but we note a slightly lower degradation at higher frequency, even if the lower deposition rate is taken into account. This could be due to better material quality due to lower ion bombardment [41], but could also be a measurement effect (the cells of both frequencies were light soaked in batches one after the other).

Figure 10 shows the *FF* and J_{sc} normalized to the first measurement, for the same cells as shown in Figure 9a. We see that the *FF* decreases strongly with increasing power. However, the slope of the degradation separates into two groups: there is a threshold power between 20 and 40 W, below which LID degradation is considerably weaker than above it.

Also, the current degradation depends strongly on the deposition power, being stronger for high power. For the solar cells deposited at 7 and 10 W, one can see a stepwise increase of the current density (marked by arrows). We suspect that the substrates detached at this moment from the cooling unit and the solar cells heated up, which leads to higher currents.

7. THE ROLE OF THE p-LAYER THICKNESS

The *p*-layer, and especially its thickness, has a tremendous influence on the degradation of *a*-Si:H solar cells. Figure 11a shows the LID of V_{oc} for solar cells with *p*-(*a*-SiC:H) layers of different thickness. The *p*-layer thickness is parametrized here by the deposition time, where 60” corresponds to about 14 nm. Details of this series and physical explanations are given elsewhere [22].

First, we note that V_{oc} increases with *p*-layer thickness for thin *p*-layers, as a minimum thickness is needed to create the built-in potential.

Second, we note that V_{oc} decreases with *p*-layer thickness for thick *p*-layers due to enhanced parasitic absorption therein (under standard measurement conditions, J_{sc} drops from 16.4 to 14.9 $\frac{mA}{cm^2}$ for 3 to 60 s deposition time). This leads to less electron-hole pair generation in the absorber layer, hence to a smaller Fermi-level splitting.

Third, we observe a light-induced V_{oc} increase for thin *p*-layers during light soaking, and a decrease for thick *p*-layers. While we attribute the V_{oc} decrease to LID of the absorber layer, we attribute the increase to LID of the *p*-layer itself [22], in contrast to other observations of increasing V_{oc} with light soaking with alternative explanations [42–46].

In Figure 11b, the V_{oc} of the solar cells shown in Figure 11a with a 3” *p*-layer is shown together with the V_{oc} of co-deposited solar cells on different substrates, for which the roughness increases from Smooth 4’ to Z2.3 0’. While V_{oc} increases in this case for the roughest substrates during light soaking, it decreases for smoother substrates. Based on simulations [22], we attribute the substrate-roughness-dependent V_{oc} change to poorer absorber layer quality on rough substrates.

The cells on substrates of varied roughness were not light soaked simultaneously. The comparison with measurements under standard conditions shows that the curve order of Smooth 4’, Z2.3 20’, and Z2.3 7’ is inverted here. Light intensity measurements show that the light intensity

was slightly lower for smoother substrates, which explains why the V_{oc} is in this case lower than expected.

8. DEGRADATION KINETICS OF POLYMORPHOUS SILICON

It was claimed in earlier studies of polymorphous silicon (*pm*-Si:H) [14,47,48] that this material degrades less during light soaking compared with standard amorphous silicon. However, in the study presented in Section 5, we could not find any specific deposition conditions where unusually low degradation could be observed except the generally lower degradation close to the amorphous-to-microcrystalline silicon transition. Note that we covered deposition conditions that were close to reported conditions for *pm*-Si:H and close to powdery regimes.

Therefore, *pm*-Si:H solar cells were deposited on LPCVD ZnO substrates. Three different types of cells were compared, choosing the buffer layer at the *p-i* interface and the bulk absorber layer as amorphous or polymorphous silicon.

Figure 12a shows the LID behavior of the V_{oc} of these cells. When *pm*-Si:H is used for the absorber and buffer layers, the V_{oc} is hardly affected during light soaking. In contrast, the V_{oc} of solar cells with *a*-Si:H as the absorber and buffer layers slightly decreases. Interestingly, the LID of V_{oc} is even stronger when a *pm*-Si:H buffer layer is used in combination with an *a*-Si:H absorber layer. The same trend shows up in *FF* in Figure 12b, where one can see that the fully polymorphous cells degrade least and the mixed cells degrade most.

A possible interpretation is that the polymorphous silicon suffers less from light-induced degradation than standard amorphous silicon. This is in agreement with specific literature on *pm*-Si:H [14,47,48] and generally observed for materials that are deposited close to the transition between *a*-Si:H and μc-Si:H (cf. Section 5). For the mixed cell, interface effects can play a major role: using a low-quality buffer layer at the *p-i* interface is more detrimental than a poor *i*-layer absorber material. Further, charge accumulation in the buffer layer in light-induced defect states can lead to a strong reduction of the electric field in the absorber layer, and hence, to strong light-induced degradation [35,36].

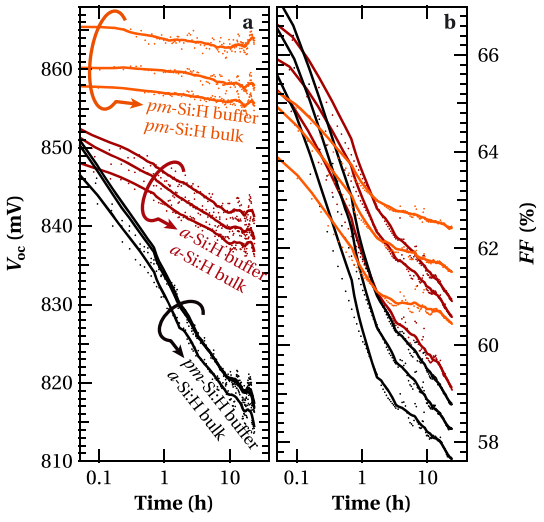

Figure 12. Open-circuit voltage (a) and fill factor (b) degradation kinetics of polymorphous and amorphous silicon solar cells produced at LPICM (Palaiseau, France).

9. CONCLUSIONS

In this contribution, we emphasized the bandgap tunability of amorphous silicon without use of other precursor gases than silane and hydrogen. We showed that, with narrow-bandgap absorber layers, 18.2 mA / cm^2 can be reached for cells with a 300-nm-thick absorber layer, and we extracted 20 mA / cm^2 from a cell with a 1000-nm-thick absorber layer at a negative bias voltage, showing the potential of very high currents with improved light management or in tandem devices. Such narrow-bandgap absorber layers are most suited for single-junction *a*-Si:H devices, in the top cell in micromorph tandem devices, or in the second cell in tandem-, triple-, or quadruple-junction thin-film silicon devices.

On the other hand, we showed high-voltage cells providing up to V_{oc} = 1.04 V or $V_{oc} \times FF$ = 739 mV in solar cells using a wide-bandgap absorber layer. These layers are most suited for the use in the top cell of triple- or quadruple-junction thin-film silicon devices.

Mapping the two-dimensional deposition parameter space of the deposition pressure and hydrogen-to-silane ratio, we covered the deposition regimes of low pressure, protocrystalline, polymorphous, and high-pressure amorphous silicon, and compared them with respect to LID of V_{oc}, *FF*, J_{sc} and efficiency.

Further, we presented systematic studies of the influence of selected deposition parameters on the kinetics of light-induced degradation of single-junction *a*-Si:H solar cells and found the following trends for relative degradation:

- *Hydrogen dilution:* The higher the better. The upper limit is given by the amorphous-to-microcrystalline transition or acceptable current density.
- *Pressure:* The influence of pressure on LID is minor. For each pressure, the hydrogen dilution close to the amorphous-to-microcrystalline transition provides similar LID. However, if comparing cells deposited at varying pressure but with fixed hydrogen dilution, stability is higher for lower pressure because of less powder production.
- *Power:* The lower the better, if the deposition temperature is not too high. The lower limit is given by plasma extinction and economical considerations of deposition rate and throughput.

DOI: 10.1002/pip

- *p-layer:* The thinner the better. The lower limit is given by the acceptable V_{oc} in degraded state. A decreasing V_{oc} during light soaking indicates that stabilized efficiency could be higher with a thinner *p*-layer—especially for rough substrates, the V_{oc} can strongly increase during light soaking for thin *p*-layers.
- *i-layer:* The thinner the better. The lower limit is given by the acceptable current density or shunt issues.
- *Excitation frequency:* No significant difference could be found, if the deposition pressure is adapted. Eventually, higher frequencies lead to slightly more stable materials.
- *Temperature:* Only a weak deposition-temperature dependence of LID was found, in slight favor of higher temperatures. The upper limit is given by hydrogen effusion.

In semi-logarithmic scale, these trends are present both in comparing initial with light-soaked state and in comparing degradation kinetics. We found that the degradation kinetics depends only weakly on time but more on deposition conditions. Within the investigated time, we did not observe a stabilization of the solar cells.

ACKNOWLEDGEMENTS

We acknowledge Léo Egger for performing part of the measurements, Nil Almat for the optimization of *p*-layers, and Sergey Abolmasov, Erik Johnson, and Pere Roca i Cabarrocas from the Laboratory of Physics of Interfaces and Thin Films (LPICM), Ecole Polytechnique, Palaiseau (France), for providing solar cells for comparison.

This work was supported in part by the Swiss Federal Office of Energy under Grant SI/500750-01, by the Competence Center Energy and Mobility, and Swisselectric Research (DURSOL project, www.dursol.ch), and by the FP7 Project "Fast Track", funded by the European Commission under Grant 283501.

REFERENCES

1. Staebler D, Wronski C. Reversible conductivity changes in discharge-produced amorphous Si. *Applied Physics Letters* 1977; **31**: 292–294
2. Shimizu T. Staebler-Wronski effect in hydrogenated amorphous silicon and related alloy films. *Japanese Journal of Applied Physics* 2004; **43**: 3257–3268
3. Zhang SB, Branz HM. Hydrogen above saturation at silicon vacancies: H-pair reservoirs and metastability sites. *Physical Review Letters* 2001; **87**: 105503
4. Smets A, Kessels W, van de Sanden M. Vacancies and voids in hydrogenated amorphous silicon. *Applied Physics Letters* 2003; **82**: 1547–1549
5. Smets A, Wronski C, Zeman M, van de Sanden M. The Staebler-Wronski effect: new physical approaches and insights as a route to reveal its origin. *Mat. Res. Soc. Symp. Proc.* 2010; **1245**: 1245-A14-02
6. Stutzmann M, Jackson WB, Tsai CC. Light-induced metastable defects in hydrogenated amorphous silicon: a systematic study. *Physical Review B* 1985; **32**: 23–47
7. Branz HM. Hydrogen collision model: quantitative description of metastability in amorphous silicon. *Physical Review B* 1999; **59**: 5098–5512
8. Matsuda A. Thin-film silicon - growth process and solar cell application. *Japanese Journal of Applied Physics* 2004; **43**: 7909–7920
9. Matsui T, Sai H, Saito K, Kondo M. Amorphous-silicon-based thin-film solar cells exhibiting low light-induced degradation. *Japanese Journal of Applied Physics* 2012; **51**: 10NB04
10. Benagli S, Borrello D, Vallat-Sauvain E, Meier J, Kroll U, Hoetzel J, Bailat J, Steinhauser J, Marmelo M, Monteduro G, Castens L. High-efficiency amorphous silicon devices on LPCVD-ZnO TCO prepared in industrial Kai^{TM}-M R&D reactor, In *24th EU PVSEC Proceedings*, Hamburg (Germany), 2009; 2293–2298.
11. Matsui T, Sai H, Suezaki T, Matsumoto M, Saito K, Yoshida I, Kondo M. Development of highly stable and efficient amorphous silicon based solar cells, In *28th EU PVSEC Proc.*, Paris (France), 2013; 2213–2217.
12. Stutzmann M, Jackson W, Tsai C. Kinetics of the Staebler-Wronski effect in hydrogenated amorphous silicon. *Applied Physics Letters* 1984; **45**: 1075–1077
13. Deng J, Rross B, Albert M, Collins R, Wronski C. Characterization of the evolution in metastable defects created by recombination of carriers generated by photo-generation and injection in pin a-Si:H solar cells. *Mat. Res. Soc. Symp. Proc.* 2006; **910**: A02-02
14. Roca i Cabarrocas P, Fontcuberta i Morral A, Poissant Y. Growth and optoelectronic properties of polymorphous silicon thin films. *Thin Solid Films* 2002; **403–404**: 39–46
15. Fontcuberta i Morral A, Roca i Cabarrocas P. Structure and hydrogen content of polymorphous silicon thin films studied by spectroscopic ellipsometry and nuclear measurements. *Physical Review B* 2004; **69**: 125–307
16. Python M, Vallat-Sauvain E, Bailat J, Dominé D, Fesquet L, Shah A, Ballif C. Relation between substrate surface morphology and microcrystalline silicon solar cell performance. *Journal of Non-Crystalline Solids* 2008; **354**: 2258–2262
17. INDEOtec, 2014. http://www.indeotec.com (Switzerland), last accessed July 20, 2014.

18. Stuckelberger M, Despeisse M, Bugnon G, Schüttauf J-W, Haug F-J, Ballif C. Comparison of amorphous silicon absorber materials: light-induced degradation and solar cell efficiency. *Journal of Applied Physics* 2013; **114**: 154509
19. Cuony P, Marending M, Alexander D, Boccard M, Bugnon G, Despeisse M, Ballif C. Mixed-phase p-type silicon oxide containing silicon nanocrystals and its role in thin-film silicon solar cells. *Applied Physics Letters* 2010; **97**: 213502
20. Despeisse M, Boccard M, Bugnon G, Cuony P, Söderström T, Parascandolo G, Stueckelberger M, Charrière M, Löfgren L, Battaglia C, Hänni S, Billet A, Ding L, Nicolay S, Meillaud F, Wyrsch N, Ballif C. Low-conductivity doped layers for improved performance of thin film silicon solar cells on highly textured substrates, In *25th EU PVSEC Proceedings*, Valencia (Spain), 2010; 2793–2797.
21. Bugnon G, Parascandolo G, Hänni S, Stuckelberger M, Charrière M, Despeisse M, Meillaud F, Ballif C. Silicon oxide buffer layer at the p-i interface in amorphous and microcrystalline silicon solar cells. *Solar Energy Materials & Solar Cells* 2014; **120**: 143–150
22. Stuckelberger M, Riesen Y, Despeisse M, Schüttauf J-W, Haug F-J, Ballif C. Light-induced V_{oc} increase and decrease in high-efficiency amorphous silicon solar cells. *Journal of Applied Physics* 2014; **116**: 094503, DOI: 10.1063/1.4894457
23. IEC. IEC (International Electrotechnical Commission) 60904-9 Ed.2: Photovoltaic devices - Part 9: solar simulator performance requirements, 2007.
24. IEC. IEC (International Electrotechnical Commission) 60904-3 Ed.2: Photovoltaic devices - Part 3: measurement principles for terrestrial photovoltaic (PV) solar devices with reference spectral irradiance data, 2006.
25. IEC. IEC (International Electrotechnical Commission) 61646 Ed.2: Thin-film terrestrial photovoltaic (PV) modules - design qualification and type approval, 2008.
26. Stuckelberger M, Perruche B, Bonnet-Eymard M, Riesen Y, Despeisse M, Haug F-J, Ballif C. Class AAA LED-based solar simulator for steady-state measurements and light soaking. *IEEE Journal of Photovoltaics* 2014; **4**(5): 1282–1287, DOI: 10.1109/JPHOTOV.2014.2335738
27. Schüttauf JW, Niesen B, Boccard M, Bugnon G, Hänni S, Niquille X, Stuckelberger M, Sculati-Meillaud F, Haug F-J, Ballif C. High-efficiency thin-film silicon triple and quadruple junction solar cells. Manuscript in preparation 2014
28. Yan B, Yang J, Guha S. Amorphous and nanocrystalline silicon thin film photovoltaic technology on flexible substrates. *Journal of Vacuum Science and Technology A* 2012; **30**: 04D108
29. Schüttauf J-W, Bugnon G, Stuckelberger M, Hänni S, Boccard M, Despeisse M, Haug F-J, Meillaud F, Ballif C. Thin-film silicon triple-junction solar cells on highly transparent front electrodes with stabilized efficiencies up to 12.8%. *IEEE Journal of Photovoltaics* 2014; **4**: 757–762
30. Green MA, Emery K, Hishikawa Y, Warta W, Dunlop ED. Solar cell efficiency tables (version 44). *Prog. Photovolt: Res. Appl.* 2014; **22**: 701–710
31. Kim S, Chung J-W, Lee H, Park J, Heo Y, Lee H-M. Remarkable progress in thin-film silicon solar cells using high-efficiency triple-junction technology. *Solar Energy Materials & Solar Cells* 2013; **119**: 26–35
32. Fischer M, Quax R, Zeman M, Smets A. Degradation kinetics of amorphous silicon solar cells processed at high pressure and its relation to the nanostructure, In *IEEE Photovoltaic Specialists Conference Proceedings*, Tampa, FL, 2013.
33. Escarré J, Söderström K, Despeisse M, Nicolay S, Battaglia C, Bugnon G, Ding L, Meillaud F, Haug F-J, Ballif C. Geometric light trapping for high efficiency thin film silicon solar cells. *Solar Energy Materials & Solar Cells* 2012; **98**: 185–190
34. Meillaud F, Billet A, Battaglia C, Boccard M, Bugnon G, Cuony P, Charrière M, Despeisse M, Ding L, Escarre-Palou J, Hänni S, Löfgren L, Nicolay S, Parascandolo G, Stuckelberger M, Ballif C. Latest developments of high-efficiency micromorph tandem silicon solar cells implementing innovative substrate materials and improved cell design. *IEEE Journal of Photovoltaics* 2012; **2**: 236–240
35. Stuckelberger M, Shah A, Krc J, Despeisse M, Meillaud F, Ballif C. Internal electric field and fill factor of amorphous silicon solar cells, In *35th IEEE Photovoltaic Specialists Conference Proceedings*, Hawaii (USA), 2010; 001569–001574.
36. Stuckelberger M, Riesen Y, Perruche B, Despeisse M, Wyrsch N, Ballif C. Charge collection in amorphous silicon solar cells: cell analysis and simulation of high-efficiency pin devices. *Journal of Non-Crystalline Solids* 2012; **358**: 2187–2189
37. Collins RW, Ferlauto AS. Advances in plasma-enhanced chemical vapor deposition of silicon films at low temperatures. *Curr. Opin. Solid-State Mater. Sci.* 2002; **6**: 425–437
38. Collins R, Ferlauto A, Ferreira G, Chen C, Koh J, Koval R, Lee Y, Pearce J, Wronski C. Evolution of microstructure and phase in amorphous, protocrystalline, and microcrystalline silicon studied by real

time spectroscopic ellipsometry. *Solar Energy Materials & Solar Cells* 2003; **78**: 143–180

39. Ding L, Stuckelberger M, Morales Masis M, Nicolay S, Ballif C. Stability of the opto-electrical properties of Zinc Oxide electrodes in thin-film silicon solar cells under light soaking. Manuscript in preparation 2014
40. Knights JC. Characterization of plasma-deposited amorphous Si:H thin films. *Japanese Journal of Applied Physics* 1979; **18**: 101–108
41. Howling AA, Dorier JL, Hollenstein C, Kroll U, Finger F. Frequency effects in silane plasmas for plasma enhanced chemical vapor deposition. *Journal of Vacuum Science and Technology A* 1992; **10**: 1080–1085
42. Lord K, Yan B, Yang J, Guha S. Light-induced increase in the open-circuit voltage of thin-film heterogeneous silicon solar cells. *Applied Physics Letters* 2001; **79**: 3800–3802
43. Yue G, Yan B, Yang J, Lord K, Guha S. Kinetics of light-induced effects in mixed-phase hydrogenated silicon solar cells. *Mater. Res. Soc. Symp. Proc.* 2003; **762**: A12.2
44. Johnson E, Dadouche F, Gueunier-Farret M, Kleider J, Roca i Cabarrocas P. Open-circuit voltage increase dynamics in high and low deposition rate polymorphous silicon solar cells. *Physica Status Solidi A* 2010; **207**: 691–694, DOI: 10.1002/pssa.200982723
45. Matsui T, 2014. MRS spring conference 2014, presentation A1.01.
46. Rech B, Beneking C, Wieder S, Wagner H. Initial and stabilized open-circuit voltage of a-Si:H solar cells: a discussion on the basis of dark I-V curves, In *14th EU PVSEC Proceedings*, Barcelona (Spain), 1997; 574–577.
47. Kim K, Johnson E, Abramov A, Roca i Cabarrocas P. Light induced electrical and macroscopic changes in hydrogenated polymorphous silicon solar cells. *EPJ Photovoltaics* 2012; **3**: 30301
48. Kim K-H, Kasouit S, Johnson E, Roca i Cabarrocas P. Substrate versus superstrate configuration for stable thin film silicon solar cells. *Solar Energy Materials & Solar Cells* 2013; **119**: 124–128